様　式　Ｃ－１９、Ｆ－１９－１、Ｚ－１９　（共通）

科学研究費助成事業　　研究成果報告書

平成　２９　年　　６　月　２７　日現在

機関番号：　１４３０１
研究種目：　研究活動スタート支援
研究期間：　2015～2016
課題番号：　１５Ｈ０６３２０

研究課題名（和文）Ultrasonic cavitation assisted fluid jet polishing

研究課題名（英文）Ultrasonic cavitation assisted fluid jet polishing

研究代表者
ブカン　アントニー（Beaucamp, Anthony）

京都大学・工学研究科・講師

研究者番号：３０７５６８３８

交付決定額（研究期間全体）：（直接経費）　　2,300,000円

研究成果の概要（和文）：超硬合金などの硬い材料の表面や，付加製造によって製造されたを超精密表面に仕上げるために，高速流体噴射研磨（FJP）の除去率を向上させることが求められている．複雑な光学表面や人工関節などのアプリケーションがある．
そこで本研究では，FJPの加工精度を維持しつつ除去率を向上させるために，超音波キャビテーションをノズル内に発生させることで気泡をジェットに添加する方法を提案した．研磨液の流れと超音波の伝播をシミュレーションし，超音波FJPが実現可能であることを確認した．さらに，超音波FJPを行うための装置を開発した．この方法では，表面粗さを悪化させることなく除去率を380%向上させることが可能である．

研究成果の概要（英文）：Fluid jet polishing is a versatile process used in super-fine finishing of complex optics and prosthetic joints. Its advantages include highly controllable sub-millimetre polishing footprints and absence of tool wear. But the very low material removal rate means that hard materials such as cemented carbides and super-alloys, used in optical surfaces and prosthetic joints, cannot be polished from a rough condition.
In this research, we proposed a new method for adding finely controlled micro-bubbles into the slurry jet by ultrasonic cavitation. Acoustic and fluid dynamics simulation confirmed that under the right conditions, cavitation bubbles generated in the nozzle can reach the surface of the workpiece before collapsing. A prototype system was fabricated, and micro-bubbles could be observed at the nozzle outlet using a high-speed camera. Polishing experiments data then showed that micro-bubbles boost removal rate by up-to 380%, without causing any degradation of the surface finish.

研究分野：　超精密研磨

キーワード：　研磨　マイクロバブル　超音波キャビテーション　除去率　表面粗さ　超精密　光学　人工関節

１．研究開始当初の背景

Fluid Jet Polishing (FJP) is a versatile process used in industry for super-fine finishing of small and complex components, in applications such as optics and medical surfaces [1,2]. Fig. 1(a) shows a photograph of the process: a slurry of water and abrasive particles is pressurized (0.2 – 2.0 MPa) and delivered through a nozzle of small outlet diameter (0.1 - 2.0 mm). The jet impinges the workpiece, generating a small polishing area. Some important advantages of this process include: (1) ability to generate sub-millimeter polishing footprints, (2) ability to reach difficult areas such as corners and cavities, and finally (3) absence of tool wear.

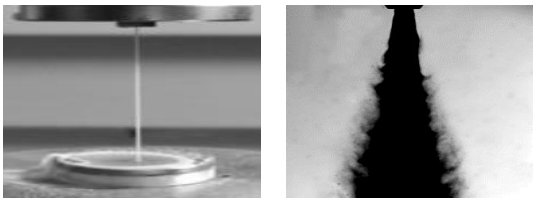

(a) Normal FJP　　(b) Air-assisted FJP

Figure 1. Jet plume comparison between normal and air-assisted FJP.

However, the main drawback of this process is its low removal rate (usually well below 1 mm3/min). There exists a correlation between pressure and grit size on the one hand and material removal rate on the other [2,3], but increasing these factors tends to strongly degrade the surface integrity of polished parts [4]. To address this issue, various concepts have been proposed from employing magnetorheological fluid [5] to making arrays of jet nozzles [6]. The main line of research has concentrated on the idea of injecting air bubbles into the FJP slurry stream, before it exits from the nozzle. Messelink et al. [7] first reported an experimental setup consisting of a pulsating air supply and mixing valve. In another attempt, Yu et al. [8] designed a nozzle inside which the Venturi effect is used to draw slurry into an air stream. In both cases, the mixing of slurry with large air bubbles was found to increase material removal rate significantly (more than 1000%). However, it also causes break-up of the jet plume, as shown in Fig. 1(b). This results in a loss of process stability, and very poor surface finish. Using the setup proposed by Messelink, low pressure (0.4 MPa) polishing comparison trials between normal and air-assisted FJP were performed on BK7 glass. The Peak-to-Valley (P-V) and Ra values, shown in Fig. 2, were found to worsen by more than 10,000%, leading to the conclusion that air-assisted FJP qualifies more as a blasting than polishing process.

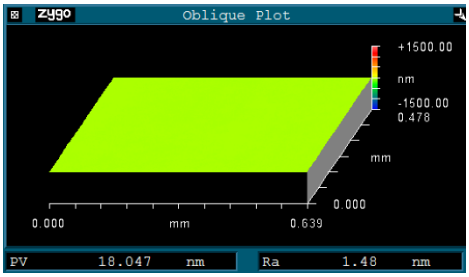

(a) Normal FJP

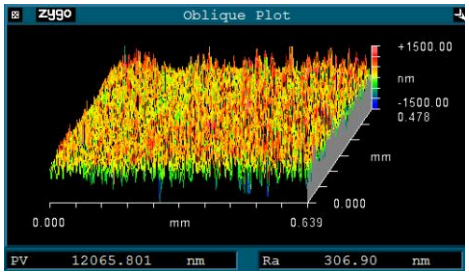

(b) Air-assisted FJP

Figure 2. Surface roughness comparison in normal and air-assisted FJP.

２．研究の目的

The main issue in previous attempts at air-assisted FJP lies with the inability to control the size and number of bubbles injected. To solve this shortcoming, a new process is proposed: “ultrasonic cavitation assisted FJP”. In this novel system, an ultrasonic transducer is attached to a specially designed nozzle cavity, and generates gas micro-bubbles within the slurry stream at a location directly upstream of the nozzle outlet. In this process, the size and number of micro-bubbles are controlled through the frequency and intensity of the ultrasonic generator. The overall design, numerical modelling, and experimental verification of a prototype system are reported. While this new process presently shows removal rates increase of only up-to 380%, our results also show that it can maintain or even improve surface roughness when compared to normal FJP.

３．研究の方法

3.1. Principle of process

The principle of ultrasonic cavitation assisted FJP is shown in Fig. 3. Slurry is injected on the side of the nozzle cavity,

and ejected from a laser-drilled sapphire outlet at the bottom, thereafter it impinges the workpiece surface. At the top, an ultrasonic transducer is affixed to a diaphragm plate, underneath which an acoustic lens is mounted. Guided by the conical shape of the cavity, acoustic waves focus upstream of the nozzle outlet.

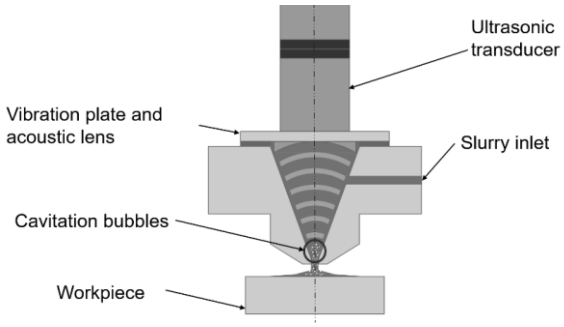

Figure 3. Principle of ultrasonic cavitation assisted FJP.

For the process to be functional, the ultrasonic equipment and nozzle cavity need to fit several criteria, as follows:

- The dimensions of the cavity should permit the generation of "standing" acoustic waves at the various operating frequencies of the transducer.
- The intensity of pressure waves at the focus point should exceed the operating FJP pressure.
- The travel time from cavitation area to workpiece should be lower than the average lifetime of micro-bubbles.

Numerical simulations were performed to assess the feasibility of this process, and derive the dimensions and specification of the cavity and ultrasonic equipment.

3.2. Numerical modelling

Numerical simulations of the ultrasonic cavitation assisted FJP process were performed with the commercially available "COMSOL" Finite Element Modelling (FEM) software. The modelling consisted of two parts: Computational Fluid Dynamics (CFD) to derive the slurry pressure and velocity in normal FJP conditions, and Acoustic Vibration Analysis (AVA) to predict the propagation of pressure waves generated by the transducer. Rotational symmetry of the system allowed simplification of the model geometry down to a 2D axi-symmetric case, as shown in Fig. 4. FEM simulation parameters are summarized in Table 1.

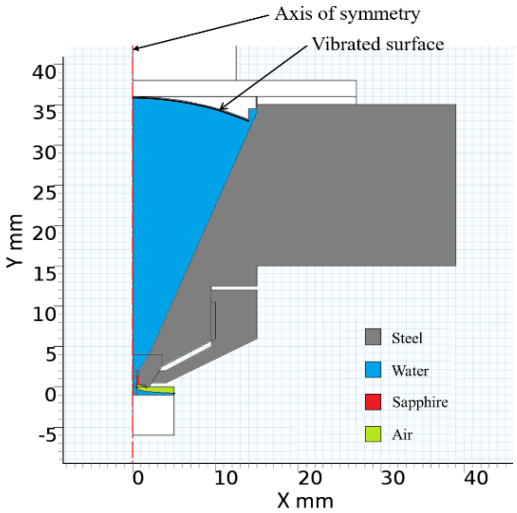

Figure 4. Geometry of the nozzle cavity in FEM software.

Table 1. Parameters of FEM simulation.

Nozzle geometry • Lens diameter • Lens radius • Outlet diameter • Stand-off distance	25 mm 35 mm 1 mm 2 mm		
Ultrasonic parameters • Frequency (kHz) • Output power (W)	26 100	78 50	130 25

3.2.1 Acoustic vibration analysis

Based on commercial availability of adequate transducers, the simulated AVA frequencies were set to 26, 78 and 130 kHz. Vibrations were applied to the axial direction of the acoustic lens surface, with the displacement acceleration a ($mm.s^{-2}$) relating to the frequency f (Hz) and intensity I ($W.m^{-2}$) of oscillations through the relationship:

$$a = 2\pi f \cdot \sqrt{\frac{2I}{Z_0}}$$

Z0 ($Pa.s.m^{-3}$) is the acoustic impedance, which is determined from the density ρ ($kg.m^{-3}$) and acoustic propagation speed c ($m.s^{-1}$) of the fluid:

$$Z_0 = \rho c$$

The intensity of oscillations I is determined from the transducer output Q (W) and surface area S (mm^2) of the acoustic lens:

$$I = \frac{Q}{S}$$

In order to obtain standing waves at all frequencies, the nozzle cavity depth was numerically optimized to a value of around 35 mm. AVA simulations, shown in Fig. 5, confirm the sustainability of standing waves by reflection inside the nozzle cavity.

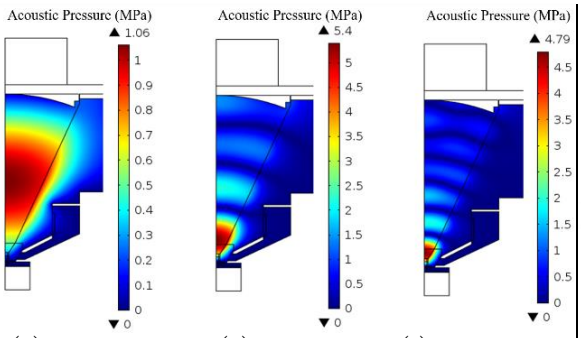

(a) 26 kHz (b) 78 kHz (c) 130 kHz

Figure 5. Simulated distribution of acoustic pressure.

For all frequencies, maximum acoustic pressure occurred on the axis of symmetry, with maximum pressure up-to 1 MPa for the lowest frequency, and up-to 5 MPa for the higher frequencies. Fig. 6 shows pressure profiles extracted along the axis of symmetry, as a function of distance from the workpiece. For standard FJP operation (up-to 2 MPa), sufficient depressurization was predicted in the case of 78 and 130 kHz. For the lowest 26 kHz frequency, applicability may be restricted to operating pressures up-to 0.9 MPa only (black horizontal line). The shortest distance to be travelled by micro-bubbles exiting the cavitation area was found to be 11, 1.6, and 1.5 mm for frequencies of 26, 78 and 130 kHz respectively.

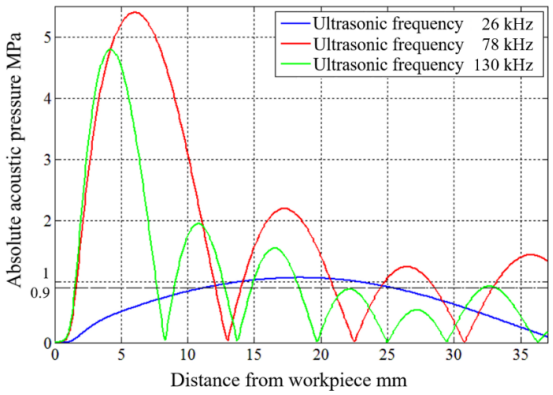

Figure 6. Pressure distribution on the axis of symmetry.

3.2.2 Computational fluid dynamics

CFD computations were performed using a dynamic multi-phase model proposed in previous publication [9]. Inlet pressure was set to 0.8 MPa and outlet to 0 MPa. Simulations produced the velocity distribution shown in Fig. 7a. Jet velocity of approximately 40 m.s^{-1} was predicted at the nozzle outlet, but fluid velocity rapidly decreases directly above the outlet. Integration of travel time as a function of distance from the workpiece is shown in Fig. 7b. This curve can be used to assess the time required for a cavitation micro-bubble to reach the surface, as a function of its onset location inside the cavity.

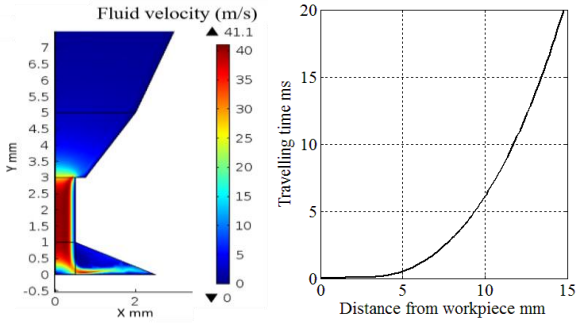

(a) Fluid velocity (b) Travel time on Y-axis

Figure 7. Simulation at 0.8 MPa pressure.

Table 2. Bubble lifetime and travel time.

Ultrasonic frequency (kHz)	26	78	130
Lifetime of bubbles (ms)	7.2	2.4	1.4
Travel time of bubbles (ms)	8.2	0.06	0.06

Observations of cavitation micro-bubbles by high-speed camera were reported in the literature by Luther et al [10]. According to this work, the average lifetime of cavitation bubbles is equal to 200 acoustic pressure cycles. Using this ratio, the average micro-bubble lifetime was assessed for the frequencies used in this project, as shown in Table 2. The integrated travel time derived from Fig. 8b is also provided. According to these simulations, it was predicted that micro-bubbles should have sufficient time to reach the workpiece surface in the case of 78 and 130 kHz. However, in the case of the lower 26 kHz it was uncertain whether bubbles would reach the workpiece, as their travel time exceeded the predicted lifetime.

3.3. Prototype system

A prototype system was assembled as shown in Fig. 8. The ultrasonic generator and transducer were sourced from industry. The acoustic lens and nozzle cavity were fabricated by precision CNC turning and milling, then assembled to a column striding a manually adjustable slide (Z-axis). An opposing column was equipped with an automated X/Y-axis stage, such that the workpiece could be moved along raster paths. During operation, the nozzle and workpiece are kept within a

waterproof silicon enclosure. Slurry is supplied by a FJP slurry management unit equipped with temperature and pressure control.

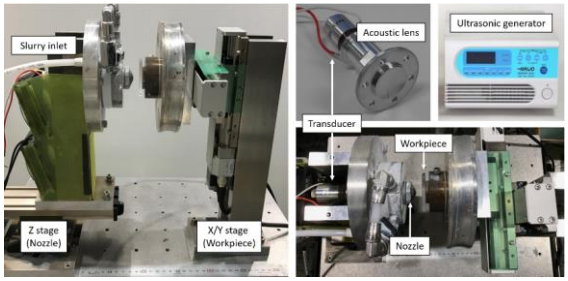

Figure 8. Prototype ultrasonic cavitation assisted FJP system.

4．研究成果

4.1. Observation of micro-bubbles

In the first set of experiments, it was verified that micro-bubbles are generated by ultrasonic cavitation and escape the nozzle. A small glass chamber was attached to the nozzle outlet and clear water was pumped through the system. A high-speed camera with zoom lens was focused on the nozzle outlet, whilst a bright light was shone from the opposite side of the chamber. The high-speed camera shutter speed was set to 3 µs, and frame rate of 6518 fps. With an inlet pressure of 0.4 MPa, this shutter speed corresponds to a fluid displacement of 60 µm from the nozzle outlet. Under these conditions, dark puffs of micro-bubbles could be seen escaping the nozzle at regular intervals, as shown in Fig 9(b) to Fig 9(d). In the case of normal FJP, shown in Fig. 9(a), only static bubbles were observed (attached to the walls of the chamber). Generation of micro-bubbles in the presence of abrasive particles was also confirmed, by running the experiment with a dilute slurry of 0.6 µm Al2O3 particles at 1 g.L^{-1} mass concentration.

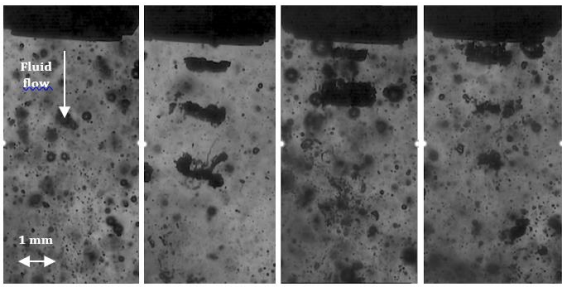

(a) No ultrasound (b) 26 kHz (c) 78 kHz (d) 130 kHz

Figure 9. Photographs of micro-bubble clouds escaping the nozzle outlet.

4.2. Material removal rate

Material removal was assessed on electroless nickel and BK7 glass samples of diameter 50 mm, by impinging at static locations on the workpiece and measuring the removed volume with a Fizeau interferometer. The experiments included: FJP pressure of 0.8 MPa, Al203 abrasives at 20 g.L^{-1} in two grit sizes (0.6 and 4.0 µm), three ultrasonic frequencies (26, 78 and 130 kHz), and three output powers (15, 30 and 50 W). The results are presented in Fig. 10 and 11. In all cases, activating the ultrasonic transducer caused an increase in material removal rate. The effect was found to be proportional to the ultrasonic output power, as shown in Fig. 10. The increase was most noticeable in the case of the finer 0.6 µm grit abrasives, with a maximum increase of 382% at 26 kHz on electroless nickel. For this grit size, the removal boost was slightly biased towards this lower frequency, but at 4.0 µm grit a strong bias towards 26 kHz (not shown here) could be observed. These observations suggest a possible correlation between abrasive size and micro-bubble size (itself linked to the ultrasonic frequency [11]).

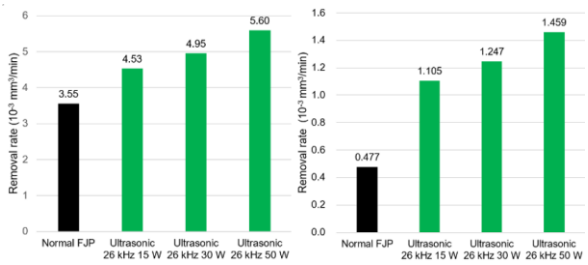

(a) Electroless nickel (b) BK7 glass

Figure 10. Material removal rate for 4.0 µm grit and 0.8 MPa.

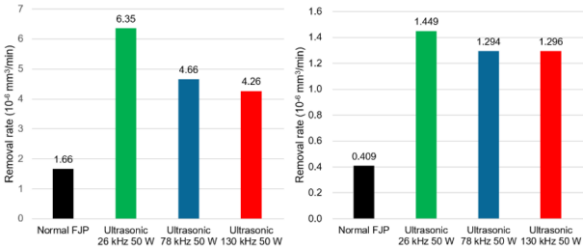

(a) Electroless nickel (b) BK7 glass

Figure 11. Material removal rate for 4.0 µm grit and 0.8 MPa.

4.3. Surface roughness

Surface roughness tests were performed by rastering square areas of the workpieces with the automated X/Y stage, while using parameters similar to those in section 3.2. Each polished area was measured at 3 locations with a 50x magnification optical profiler. The results presented in Fig. 12 show that in all cases roughness was either maintained, or

slightly improved.

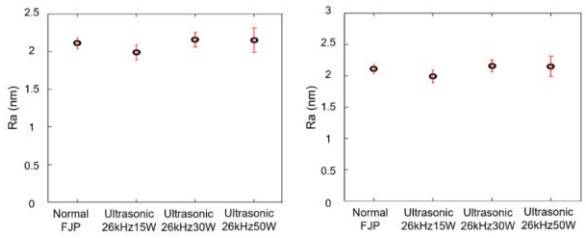

(a) Electroless nickel (4.0μm) (b) BK7 glass (4.0μm)

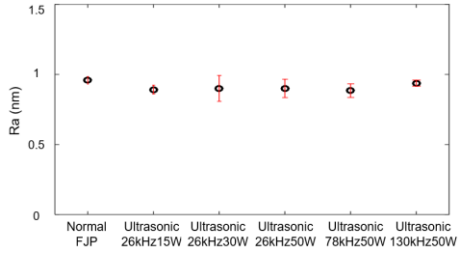

(c) Electroless nickel (0.6 μm grit)

Figure 12. Surface roughness (50x) at 0.8 MPa pressure

4. 4. Summary

As expected, basic polishing trials confirmed material removal rate increases of up-to 380%, while maintaining or even slightly improving the surface roughness. The experimental results suggest a possible correlation between removal rate, grit and micro-bubble size.

５．主な発表論文等

〔雑誌論文〕（２）

(1) Beaucamp A., Katsuura T., Kawara Z., A novel ultrasonic cavitation assisted fluid jet polishing system, CIRP Annals–Manufacturing Technology, 66/1, 2017, 1-4
https://doi.org/10.1016/j.cirp.2017.04.083

(2) Beaucamp A., Simon P., Charlton P., King C., Matsubara A., Wegener K., Brittle-ductile transition in shape adaptive grinding (SAG) of SiC aspheric optics, International Journal of Machine Tools and Manufacture, 115, 2017, 29-37.
https://doi.org/10.1016/j.ijmachtools.2016.11.006

〔学会発表〕（３）

(1) 勝浦知也, Beaucamp Anthony, 松原厚, 超音波キャビテーションを利用した高速流体噴射研磨, 2016 年度精密工学会春季大会, 茨城大学.

(2) Walker D., Yu G., Beaucamp A., Bibby M., Li H., McCluskey L., Petrovic S., Reynolds C., More steps towards process automation for optical fabrication, Fourth European Seminar on Precision Optics Manufacturing, International Society for Optics and Photonics, 2017, Deggendorf, Germany.

(3) Beaucamp A., Process modelling for super-fine finishing of carbides, First conference on physical modelling for virtual manufacturing systems and processes, 2017, Speyer, Germany.

〔図書〕
なし
〔産業財産権〕
なし
〔その他〕
なし

６．研究組織

(1)研究代表者
ブカンアントニータデスエルヴぇ
(BEAUCAMP, Anthony, Tadeus, Herve)
京都大学・大学院工学研究科・講師
研究者番号： ３０７５６８３８

(2)研究分担者
なし

(3)連携研究者
なし

(4)研究協力者
勝浦 知也 (KATSUURA, Tomoya)
京都大学・大学院工学研究科・修士課程

References

[1] Fähnle, O., Brug, H., Frankena, H., 1998, Fluid jet polishing of optical surfaces, Applied Optics, 37:6771-6773.

[2] Beaucamp, A., Namba, Y., 2013, Super-smooth finishing of diamond turned hard X-ray molding dies by combined fluid jet and bonnet polishing, Annals of the CIRP, 62/1:315-318.

[3] Fang, H., Guo, P., Yu, J., 2006, Surface roughness and material removal in fluid jet polishing, Applied Optics, 45/17:4012-4019.

[4] Beaucamp, A., Namba, Y., Messelink, W., Walker, D., Charlton, P., Freeman, R., 2014, Surface integrity of fluid jet polished tungsten carbide, Proc. CIRP, 13:377-381.

[5] Tricard, M., Kordonski, W., Shorey, A., Evans, C., 2006, Magnetorheological Jet Finishing of Conformal, Freeform and Steep Concave Optics, Annals of the CIRP, 55/1:309-340.

[6] Wang, C., Cheung, C., Ho, L., Liu, M., Lee, W., 2017, A novel multi-jet polishing process and tool for high-efficiency polishing, International Journal of Machine Tools and Manufacture, 115:60-73.

[7] Messelink, W., Faehnle, O., 2008, Exploiting the process stability of fluid jet polishing, Optical Fabrication and Testing, OSA Technical Digest, pp. OThD3.

[8] Yu, Z., Kuo, C., Chen, C., Hsu, W., Tsai, P., 2011, Study of air-driving fluid jet polishing, Proc. of SPIE, 8126:1–6.

[9] Beaucamp, A., Namba, Y., Freeman, R., 2012, Dynamic multiphase modelling and optimization of fluid jet polishing process, Annals of the CIRP, 61/1:315-318.

[10] Luther, S., Mettin, R., Koch, P., Lauterborn, W., 2001, Observation of acoustic cavitation bubbles at 2250 frames per second, Ultrasonic Sonochemistry, 8:159-162.

[11] Brotchie, A., Grieser, F., Ashokkumar, M., 2009. Effect of power and frequency on bubble-size distributions in acoustic cavitation, Phys. Rev. Letters, 102/8:084302.